Journal of Holography Applications in Physics
Volume 6, Issue 3, Summer 2026, 31–51
©Available online at http://jhap.du.ac.ir
DOI: 10.22128/jhap.2026.3169.1170
Online ISSN: 2783–3518

**Regular article**

# Holographic Generation of Bessel–Gaussian Vortex Beams Using a Ring–Apertured Fork Grating and Topological Charge Measurement via an Astigmatic Grating

Somaye Fathollazade[1] · Saifollah Rasouli[1,2] · Pouria Amiri[1] · Ahmad Absanov Abdusattarovich[3]

[1] Department of Physics, Institute for Advanced Studies in Basic Sciences (IASBS), Zanjan 45137–66731, Iran;
E-mail: s.fathollazade@iasbs.ac.ir
Corresponding Author E-mail: rasouli@iasbs.ac.ir
E-mail: p.amiri@iasbs.ac.ir
[2] Optics Research Center, Institute for Advanced Studies in Basic Sciences (IASBS), Zanjan 45137–66731, Iran.
[3] Engineering Physics Institute, Samarkand State University, Samarkand 703004, Uzbekistan;
E-mail: absanovakhmad@gmail.com

**Received:** November 29, 2025; **Revised:** January 10, 2026; **Accepted:** January 29, 2026

**Abstract.** In this work, we introduce a holography-based method for generating Bessel–Gaussian vortex beams (BGVBs). The approach embeds a helical phase into a diffraction grating and then applies a ring-shaped transmission function. Embedding the helical phase converts the structure into a fork grating, while multiplication by the ring aperture ensures that the vortex beam produced in the first diffraction order evolves into a BGVB in the far field. The proposed holographic element was fabricated on a glass substrate using lithography, and illumination with a Gaussian beam of suitable waist generated a clear BGVB in the first diffraction order. The measured intensity profile shows excellent agreement with theoretical predictions. To determine the topological charge (TC), we employed an astigmatic grating with locally parallel grooves exhibiting second-order curvature. Introducing astigmatic aberration at an appropriate propagation distance produces elongated intensity fringes, and counting these fringes allows accurate determination of the TC. Numerical simulations and experimental measurements exhibit strong consistency, confirming the effectiveness of the proposed method.

**Keywords**: Holography–Based Method; Bessel–Gaussian Vortex Beams (BGVBs); Helical Phase; Topological Charge (TC); Astigmatic Grating.

# Contents

# 1 Introduction

Singular optics is a branch of modern physical optics that investigates phase and polarization singularities in optical wavefields, encompassing phenomena such as optical vortices in scalar fields and polarization singularities in vector fields [1]. This field plays a crucial role in various applications, including free-space optical communications [2], optical imaging [3], optical manipulation [4], and laser-matter interactions [5].

Bessel beams constitute a fundamental class of non-diffracting optical beams and can be generated experimentally through several methods. A zeroth-order Bessel beam, characterized by a bright central core surrounded by concentric rings and no phase singularity, is typically produced by illuminating an annular aperture placed in the focal plane of a lens [11], by passing a collimated Gaussian beam through an axicon [12], or using holographic elements with an axicon-like transmission function [13]. By adding an azimuthal phase term $\exp(i\ell\phi)$, where $\ell$ is the integer topological charge (TC), the central bright spot is replaced by a dark core, transforming the beam into a Bessel–Gaussian vortex beam (BGVB) that exhibits a helical wavefront, and a ring-shaped intensity profile while preserving the non-diffracting propagation property [6,7]. These structured-light BGVBs have found widespread applications, including quantum entanglement of photons [8], underwater three-dimensional imaging [9] and optical engineering [10].

In this work, we propose and demonstrate a holographic approach for generating BGVBs. The method is based on encoding a helical phase distribution within an amplitude grating, which is then multiplied by a ring-shaped transmission function. The incorporation of the helical phase transforms the grating into a fork grating, while the ring-shaped function ensures the generation of a Bessel-type beam in the far field under plane-wave illumination. Since both functions are integrated into a single holographic structure, the first diffraction order in the far field exhibits the characteristic intensity and phase profile of a BGVB. The proposed structure was fabricated on a glass substrate using lithography, and illumination with a Gaussian beam of appropriate waist resulted in a BGVB in the first diffraction order.

In contrast to two-step techniques for generating such beams-where Laguerre-Gaussian (LG) beams are converted into BGVBs using axicons or ring-shaped structures [17,22], the proposed method offers a compact, single-step, and cost-effective solution. One practical limitation of our approach is the reduced output power due to light passing through the ring aperture; however, this issue can be largely mitigated by fabricating the hologram on a glass substrate and employing high-power lasers.

Determining the TC of vortex beams is of great importance since it plays a fundamental role in numerous applications involving orbital angular momentum (OAM). Several techniques have been developed to measure the TC of optical vortices, including interference with the beam's mirror image [16], diffraction through specially shaped apertures [18–20], and diffraction by gratings [21,23,24].

In our previous studies, an amplitude linear grating with a quadratic curvature in its grooves was employed for characterizing LG beams [25] and analyzing the axial interference of two LG beams with different TCs and zero radial indices [26]. This structure was also utilized for characterizing LG beams with nonzero radial indices [27]. Since this grating introduces astigmatic aberration into the incident wavefront, it is hereafter referred to as the *astigmatic grating*. Building upon this framework, we have recently employed the same grating for measuring the TC of LG beams and determining the optimal conditions for Laguerre-to-Hermite (LG-to-HG) mode conversion in the presence of astigmatism [28].

In the present study, the astigmatic grating is used to determine the TC of the generated BGVBs through diffraction analysis. The optimal propagation distance between the

diffraction and grating planes is theoretically derived as a function of the gratings geometric parameters and the incident beam characteristics, and then verified experimentally. The obtained experimental results show excellent agreement with both theoretical predictions and numerical simulations.

## 2 Theoretical Background of Fraunhofer Diffraction of a Gaussian Beam by a Ring-Fork grating Hologram

The transmission function of the Ring-fork grating (RFG) hologram in polar coordinates $(r'', \theta'')$ is defined as:

$$t_{RFG}(r'', \theta'') = \int_{a}^{a+s} \frac{1}{2\pi r''} \delta(r'' - r_0) dr_0 \sum_{m=-\infty}^{+\infty} t_m \, e^{-im(\frac{2\pi}{d} r'' \cos\theta'' - l\theta'')}, \tag{2.1}$$

where $t_m$, $a$, $s$, $d$, and $l$ denote the $m$th Fourier coefficient, inner radius of the ring, radial width of the ring, period of the linear fork grating, and its TC, respectively, and $\delta(\cdot)$ is the Dirac delta function. This structure is formed by multiplying the transmission function of a fork grating by that of an annular ring. The ring transmission function is constructed from the unit transmission function, mathematically represented by integrating the delta function over the interval between the ring's inner and outer radii. It is worth noting that diffraction of a plane wave by an aperture with a delta transmission function produces an ideal Bessel beam in the far field [30]. However, practically generating an ideal Bessel beam is impossible because the delta function has an infinitesimally narrow width, making fabrication challenging and the transmitted energy negligibly small. Figure 1(a) shows the transmittances of the ring and fork gratings, and the resulting structure, the RFG hologram. Next, we compute far-field diffraction of a Gaussian beam incident on this structure.

When a beam with transmission function $U(r'', \theta'', z' = -0)$ passes through the RFG hologram, the complex amplitude of the transmitted field immediately after the structure is given by:

$$U(r'', \theta'', z' = +0;) = t_{RFG}(r'', \theta'') U(r'', \theta'', z' = -0), \tag{2.2}$$

where $-0$ and $+0$ denote the positions immediately before and after the structure, respectively. Substituting the RFG hologram transmission function from equation (2.1) and assuming the incident beam is a Gaussian beam, the complex amplitude immediately after the RFG hologram at $z' = +0$ becomes:

$$U(r'', \theta'', z' = +0) = e^{-\frac{r''^2}{w_0^2}} \int_{a}^{a+s} \frac{1}{2\pi r''} \delta(r'' - r_0) dr_0 \tag{2.3}$$
$$\times \sum_{m=-\infty}^{+\infty} t_m \, e^{-im\left(\frac{2\pi}{d} r'' \cos\theta'' - l\theta''\right)}.$$

The complex amplitude of the beam after Fraunhofer diffraction from the structure at a propagation distance $z'$ is calculated using the following equation, [20]:

$$U(r', \theta', z') = h \int_{0}^{+\infty} \int_{0}^{2\pi} U(r'', \theta'', z' = +0) \exp\left(-i2\alpha r' r'' \cos(\theta'' - \theta')\right) r'' dr'' d\theta'', \tag{2.4}$$

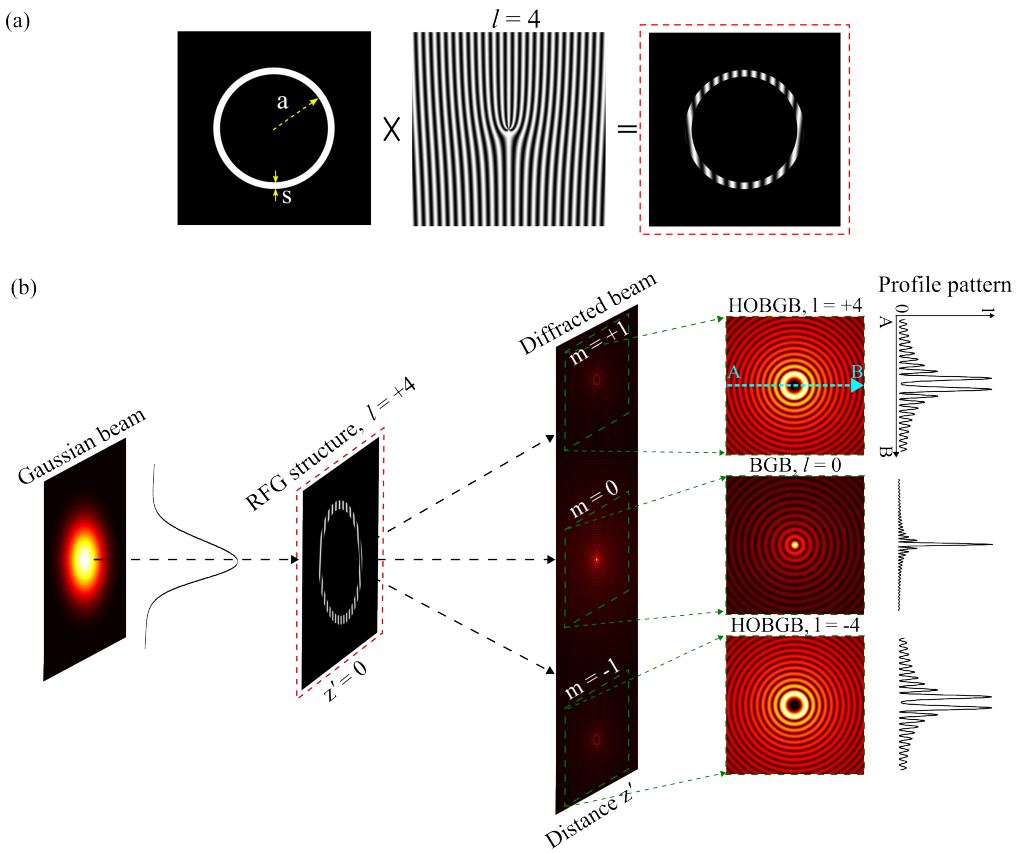


Figure 1: (a) Hologram generated by multiplying a ring of width $s = 0.1$ mm and inner radius $a = 3$ mm with a fork grating of TC $l = 4$ and $d = 0.1$ mm. (b) Schematic setup for generating BGVBs by passing a Gaussian beam through an amplitude RFG hologram. Parameters: incident beam waist $w_0 = 2.5$ mm, and diffraction pattern recorded at $z' = 2$ m.

where

$$h = \frac{\exp(ikz')}{i\lambda z'} \times \exp(i\alpha r'^2), \quad \alpha = \frac{\pi}{\lambda z'},$$

with $\lambda$ the wavelength and $k = \frac{2\pi}{\lambda}$ the wave number. By substituting Eq. (2.3) into Eq. (2.4), we get:

$$U(r', \theta', z') = h \int_a^{a+s} \int_0^{+\infty} \int_0^{2\pi} e^{-\frac{r''^2}{w_0^2}} \frac{1}{2\pi r''} \delta(r'' - r_0) \tag{2.5}$$

$$\times \sum_{m=-\infty}^{+\infty} t_m \, e^{-im\left(\frac{2\pi}{d} r'' \cos\theta'' - l\theta''\right)} e^{-2i\alpha r' r'' \cos(\theta'' - \theta')} r'' dr'' d\theta'' dr_0.$$

Using the delta function property, equation Eq. (2.5) simplifies to:

$$U(r',\theta',z') = \tfrac{h}{2\pi} \int_{a}^{a+s} e^{-\frac{r_0^2}{w_0^2}} \times \int_0^{2\pi} \sum_{m=-\infty}^{+\infty} t_m\, e^{-im\left(\frac{2\pi}{d} r_0 \cos\theta'' - l\theta''\right)} e^{-2i\alpha r' r_0 \cos(\theta''-\theta')} d\theta'' dr_0. \tag{2.6}$$

By defining $\kappa_m = m\frac{2\pi}{d}$ and separating the summation into the $m = 0$ term and the positive and negative $m$ terms, the complex amplitude of the field is expressed as follows:

$$\begin{aligned} U(r',\theta',z') = h \int_a^{a+s} e^{-\frac{r_0^2}{w_0^2}} \Bigg[ & \tfrac{t_0}{2\pi} \int_0^{2\pi} e^{-2i\alpha r' r_0 \cos(\theta''-\theta')} d\theta'' \\ & + \sum_{m=1}^{+\infty} \tfrac{t_m}{2\pi} \int_0^{2\pi} e^{-2i\alpha r_0 \cos\theta''(r'\cos\theta' + \frac{\kappa_m}{2\alpha})} e^{iml\theta''} e^{-2i\alpha r_0 \sin\theta'' r' \sin\theta'} d\theta'' \\ & + \sum_{m=1}^{+\infty} \tfrac{t_{-m}}{2\pi} \int_0^{2\pi} e^{-2i\alpha r_0 \cos\theta''(r'\cos\theta' - \frac{\kappa_m}{2\alpha})} e^{-iml\theta''} e^{-2i\alpha r_0 \sin\theta'' r' \sin\theta'} d\theta'' \Bigg] dr_0. \end{aligned} \tag{2.7}$$

By applying the variable transformations $(r'\cos\theta' \pm \frac{\kappa_m}{2\alpha}) = r'_{\pm m}\cos\theta'_{\pm m}$ and $r'\sin\theta' = r'_{\pm m}\sin\theta'_{\pm m}$[29], we obtain:

$$\begin{aligned} U(r',\theta',z') = h \int_a^{a+s} e^{-\frac{r_0^2}{w_0^2}} \Bigg[ & \tfrac{t_0}{2\pi} \int_0^{2\pi} e^{-2i\alpha r' r_0 \cos(\theta''-\theta')} d\theta'' \\ & + \sum_{m=1}^{+\infty} \tfrac{t_m}{2\pi} \int_0^{2\pi} e^{-2i\alpha r_0 \cos\theta'' r'_{+m}\cos\theta'_{+m}} e^{iml\theta''} e^{-2i\alpha r_0 \sin\theta'' r'_{+m}\sin\theta'_{+m}} d\theta'' \\ & + \sum_{m=1}^{+\infty} \tfrac{t_{-m}}{2\pi} \int_0^{2\pi} e^{-2i\alpha r_0 \cos\theta'' r'_{-m}\cos\theta'_{-m}} e^{-iml\theta''} e^{-2i\alpha r_0 \sin\theta'' r'_{-m}\sin\theta'_{-m}} d\theta'' \Bigg] dr_0, \end{aligned} \tag{2.8}$$

where $r'_{\pm m} = \sqrt{r'^2 + (\frac{\kappa_m}{2\alpha})^2 \pm \frac{\kappa_m r'\cos\theta'}{\alpha}}$ and $\tan\theta'_{\pm m} = \frac{r'\sin\theta'}{r'\cos\theta' \pm \frac{\kappa_m}{2\alpha}}$, which are related to the beam parameters in the observation plane. After some simplification we have

$$\begin{aligned} U(r',\theta',z') = h \int_a^{a+s} e^{-\frac{r_0^2}{w_0^2}} \Bigg[ & \tfrac{t_0}{2\pi} \int_0^{2\pi} e^{-2i\alpha r' r_0 \cos(\theta''-\theta')} d\theta'' \\ & + \sum_{m=1}^{+\infty} \tfrac{t_m}{2\pi} \int_0^{2\pi} e^{iml\theta''} e^{-2i\alpha r_0 r'_{+m}\cos(\theta''-\theta'_{+m})} d\theta'' \\ & + \sum_{m=1}^{+\infty} \tfrac{t_{-m}}{2\pi} \int_0^{2\pi} e^{-iml\theta''} e^{-2i\alpha r_0 r'_{-m}\cos(\theta''-\theta'_{-m})} d\theta'' \Bigg] dr_0. \end{aligned} \tag{2.9}$$

The complex amplitude of the beam at the propagation distance $z'$, by applying the integral describing the Bessel function of the first kind from reference [31],

$$\frac{1}{2\pi} \int_0^{2\pi} e^{il\gamma} e^{-ix\cos\gamma} d\gamma = i^l J_l(x),$$

is rewritten as follows:

$$\begin{aligned} U(r',\theta',z') = h \int_a^{a+s} e^{-\frac{r_0^2}{w_0^2}} \Big[ & t_0 J_0(2\alpha r_0 r') \\ & + \sum_{m=1}^{+\infty} t_m i^{ml} J_{ml}(2\alpha r_0 r'_{+m}) e^{iml\theta'_{+m}} + \sum_{m=1}^{+\infty} t_{-m} i^{-ml} J_{-ml}(2\alpha r_0 r'_{-m}) e^{-iml\theta'_{-m}} \Big] dr_0. \end{aligned} \tag{2.10}$$

The terms $e^{\pm iml\theta'_{\pm m}}$ that appear in the nonzero diffraction orders indicate that the TC of the beams generated in these orders is scaled by the factor $m$. In other words, the TC varies as $l \times m$.

Equation (2.10) can be separated into:

$$U(r', \theta', z') = \int_a^{a+s} U_0(r', \theta', z'; r_0) dr_0 \tag{2.11}$$
$$+ \int_a^{a+s} \sum_{m=1}^{+\infty} (U_{+m}(r'_{+m}, \theta'_{+m}, z'; r_0) + U_{-m}(r'_{-m}, \theta'_{-m}, z'; r_0)) dr_0,$$

where the first term corresponds to the zero-order Bessel-Gaussian beam, and the subsequent terms correspond to BGVBs. The intensity distribution of the generated beam is given by $I(r', \theta', z') = U(r', \theta', z')U^*(r', \theta', z')$, where $^*$ denotes complex conjugation. Figure 1(b) shows the far-field diffraction pattern of a Gaussian beam passing through a sinusoidal-profile RFG hologram. For the sinusoidal profile in Eq. (2.10), Fourier coefficients are $t_0 = \frac{1}{2}$ and $t_{\pm m} = \frac{1}{4}$. The ring radius $r_0$, ring width $s$, and TC $l$ are 1 mm, 0.1 mm, and 4, respectively. The fork grating period is $d = 0.1$ mm, and the Gaussian incident beam waist is $w_0 = 2.5$ mm. The diffraction pattern is recorded at a propagation distance $z' = 2$ m. Figure 2 illustrates the effect of the RFG hologram's inner radius $r_0$ and ring width $s$ on the quality of the generated BGVBs. As shown, increasing the width $s$ reduces the number of rings surrounding the central ring in the intensity distribution of the generated beam. Conversely, increasing the inner radius $r_0$ decreases the overall size of the generated BGVB. The theoretical results derived from equation (2.10) are shown in gray color map, while the Gaussian beam diffraction simulations from the RFG hologram are shown with the hot colormap. Odd rows present one-dimensional (1D) intensity profiles crossing the center (indicated by red dashed lines in the first row, first column). Parameters for this figure include a TC of $l = 5$ and an incident Gaussian beam waist $w_0 = 1$ mm. The diffraction patterns correspond to a propagation distance of $z' = 2$ m. Generally, increasing ring width $s$ not only reduces the number of rings around the central ring but also introduces a halo around the generated beam, thereby reducing beam quality.

Figure 3 shows the propagation behavior of BGVBs with TC $l = 5$, generated by RFG holograms with inner radii $r_0 = 0.5$ mm and 1 mm, and widths $s = 0.05$ mm and 0.2 mm at different propagation distances $z'$. Results indicate that for structures with larger ring widths, increasing the propagation distance effectively reduces the halo surrounding the beam. This means that at larger propagation distances, the ring diffraction effects become more similar to those of the ideal delta function diffraction, improving the quality of the generated beam. As in Figure 2, the first and last columns show theoretical results from equation 2.10, while the middle columns present simulation results. The comparison clearly demonstrates good agreement between theory and simulation.

# 3 Theoretical Basis for Determining the Optimal Propagation Distance for Characterizing BGVBs under Astigmatic Aberration

In this section, the theoretical foundation for determining the optimal propagation distance required for characterizing BGVBs in the presence of astigmatic aberration is presented.

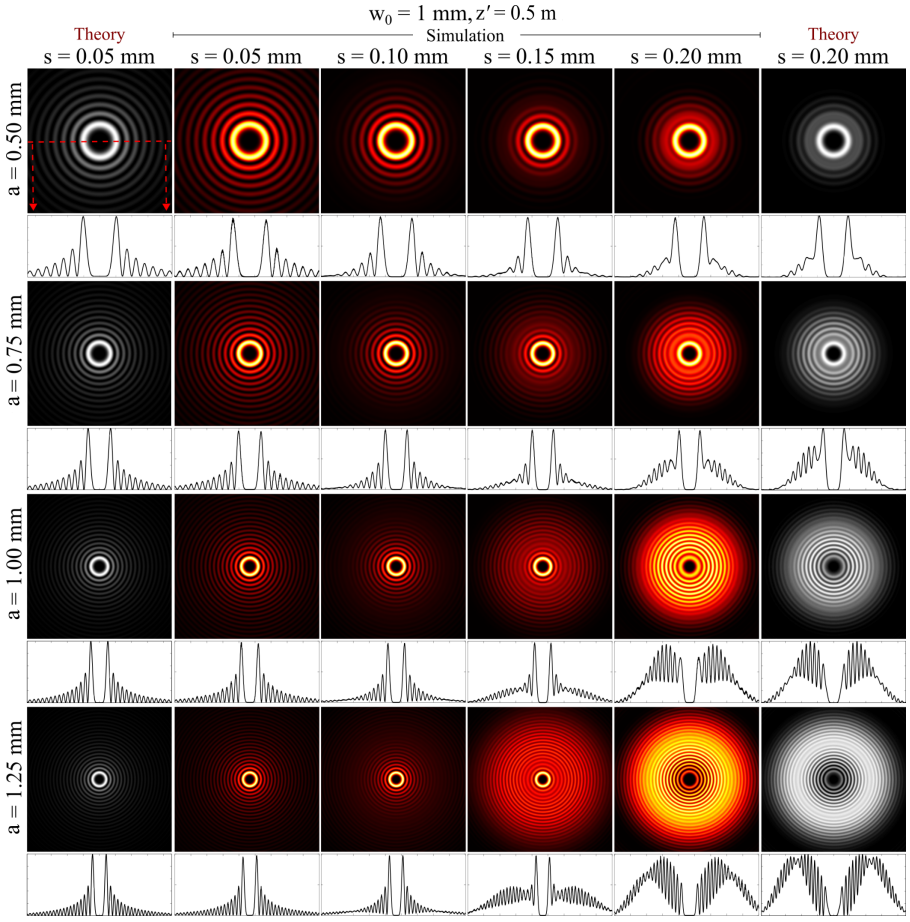


Figure 2: Effect of the RFG hologram inner radius ($a$) and ring width ($s$) on the quality of generated BGVBs. Parameters: TC $l = 5$, incident Gaussian beam waist $w_0 = 1$ mm, and propagation distance $z' = 0.5$ m.

The complex amplitude of a BGVB at the initial plane $z = 0$ is defined as [4]:

$$U_{\mathrm{BGVB}}(r', \theta', z = 0) = J_l\left(\frac{r'}{w_b}\right) \exp(il\theta') \exp\left(-\frac{r'^2}{w_{0B}^2}\right), \tag{3.1}$$

where $J_l(.)$ is the Bessel function of order $l$, $w_{0B}$ denotes the Gaussian envelope width, and $w_b$ represents the Bessel scale parameter. The variable $\theta'$ indicates the azimuthal angle in polar coordinates. According to Eq. 22.15.2 of Ref. [32], when the radial index $p$ of the LG modes is large, the Bessel function of the first kind can be approximated using the generalized Laguerre polynomial as:

$$J_l(X) \approx \left(\frac{X}{2p}\right)^l {L_p}^l\left(\frac{X^2}{4p}\right), \quad \text{for a large value of } p. \tag{3.2}$$

Here, $L_p^l(.)$ is the generalized Laguerre polynomial of radial index $p$ and TC $l$. By applying this approximation, Eq. (3.1) can be rewritten, showing that the BGVB becomes equivalent

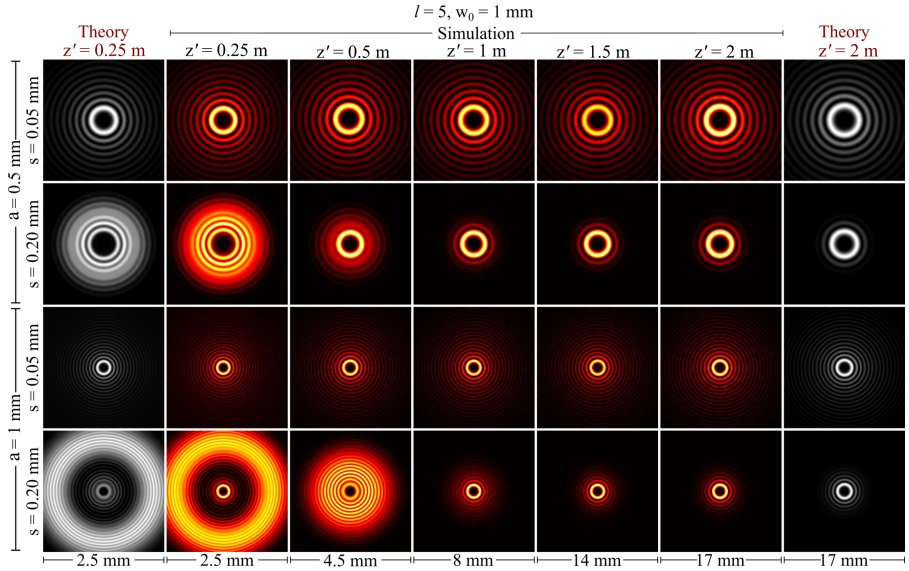


Figure 3: Propagation of BGVBs with TC $l = 5$, generated by RFG holograms with two different inner radii and ring widths, at various propagation distances.

to its corresponding LG beam:

$$U_{\mathrm{BGVB}}(r', \theta', z = 0) = \left(\frac{r'}{2pw_b}\right)^l L_p{}^l\left(\frac{r'^2}{4pw_b^2}\right) \exp(il\theta') \exp\left(-\frac{r'^2}{w_{0B}^2}\right). \tag{3.3}$$

The complex amplitude of an LG beam in polar coordinates is given by [33]:

$$\mathcal{L}_p^l(r/w_{0LG}) = \exp\left(-\frac{r^2}{w_{0LG}^2}\right)\left(\frac{r}{w_{0LG}}\right)^{|l|} \exp(il\theta) L_p^l\left(\frac{2r^2}{w_{0LG}^2}\right). \tag{3.4}$$

By comparing Eqs. (3.3) and (3.4), the following condition is obtained:

$$w_{0LG}^2 = 8p\, w_b^2.$$

Satisfying this condition ensures that most of the bright and dark rings of both beams spatially overlap. As the value of $p$ increases, the degree of overlap improves, resulting in a larger number of coinciding bright and dark rings. Consequently, Eq. (3.3) can be simplified as:

$$U_{\mathrm{BGVB}}(r', \theta', z = 0) = \left(\frac{2}{p}\right)^{l/2} \mathcal{L}_p^l\left(\frac{r'}{w_{0LG}}\right). \tag{3.5}$$

This result indicates that, by setting $w_{0LG} = \sqrt{8p}\, w_b$, the complex amplitude of a BGVB becomes equivalent-up to a constant factor $\left(\frac{2}{p}\right)^{l/2}$-to that of an LG beam with a very large radial index $p$. Figure 4 compares the intensity distributions of the two beams. As $p$ increases, the similarity between the intensity profiles becomes more pronounced, and the bright and dark rings nearly coincide.

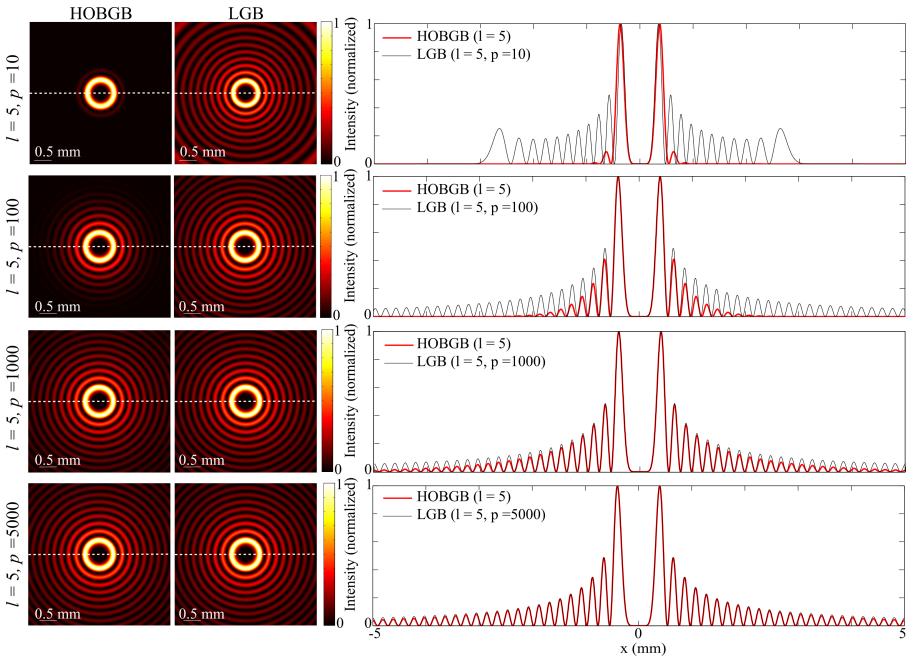


Figure 4: Comparison between BGVBs and LG beams with different radial indices to illustrate the effect of the radial index on their structural similarity. For both beams, the TC is set to $l = 5$, and the beam widths are selected according to the approximation $8p{w_b}^2 = {w'_{0LG}}^2$ with $w_b = 0.06$ mm.

This approximation allows the theoretical relations developed for LG beams under astigmatism [28] to be extended to BGVBs, provided that the beam parameters are defined as $w_0 = w_{0LG}$ and the Rayleigh length as $z_R = \pi w_{0LG}^2/\lambda$.

Astigmatic aberration in an optical wavefront is defined as the difference in curvature between the $x$- and $y$-directions [34]. At the plane $z = +0$, where the BGVB passes through an astigmatic element, the complex amplitude of the field in Cartesian coordinates is expressed as:

$$U_{\mathrm{BGVB}}(x', y', z = +0) = \left(\frac{2}{p}\right)^{l/2} \times \exp\left[i\left(c_x \frac{x'^2}{w_{0LG}^2} + c_y \frac{y'^2}{w_{0LG}^2}\right)\right] \mathcal{L}_p^l\left(\frac{\sqrt{x'^2 + y'^2}}{w_{0LG}}\right), \quad (3.6)$$

where $c_x$ and $c_y$ are dimensionless astigmatism parameters. The constant factor $\left(\frac{2}{p}\right)^{l/2}$ originates from the Bessel-to-Laguerre approximation and remains unchanged during propagation.

Using the propagation relation of an astigmatically aberrated beam given in Eq. (15) of Ref. [28], the propagated field after a distance $z$ can be written as:

$$U_{\mathrm{BGVB}}(r', \theta', z) \propto \left(\frac{2}{p}\right)^{l/2} \gamma w_x w_y e^{i\gamma r^2} e^{-\gamma^2(w_x^2 x^2 + w_y^2 y^2)} \times \quad (3.7)$$
$$\sum_{n=0}^{p} \sum_{m=0}^{|l|} c_{m,n}^{\pm} e^{i(n_1\phi_x + n_2\phi_y)} H_{n_1}\left(\sqrt{2\gamma|w_x|^2}\,\frac{x}{w_{0LG}}\right) H_{n_2}\left(\sqrt{2\gamma|w_y|^2}\,\frac{y}{w_{0LG}}\right),$$

where

$$n_1 = |l| + 2n - m, \qquad n_2 = 2p - 2n + m,$$

and the parameters are defined as:

$$w_x = \frac{w_{0LG}}{\sqrt{1 - i(c_x + z_R/z)}}, \quad w_y = \frac{w_{0LG}}{\sqrt{1 - i(c_y + z_R/z)}},$$
$$\phi_x = \arctan(c_x + z_R/z), \quad \phi_y = \arctan(c_y + z_R/z),$$
$$\gamma = \frac{\pi}{\lambda z}.$$

These results indicate that, similar to LG beams, it is possible to determine an optimal propagation distance TC retrieval in BGVBs. According to Eq. (14) of Ref. [28], mode conversion occurs when the astigmatism parameters $c_x$ and $c_y$ satisfy the following condition:

$$(1 + c_x c_y)\zeta^2 + (c_x + c_y)\zeta + 1 = 0, \tag{3.8}$$

where $\zeta = z/z_R$ and $z_R = \pi w_{0LG}^2/\lambda$. It should be noted that, for LG beams in this scenario, mode conversion to HG modes and TC retrieval are equivalent processes. However, in the case of BGVBs at the optimal propagation distance, diffraction produces a pattern well-suited for measuring the TC from the intensity profile. Full conversion of BGVBs to HG modes is not achievable, because the corresponding HG mode would require an infinite radial index $p$; given finite spatial resolution, complete conversion is impossible within a bounded region. Solving Eq. (3.8) yields the propagation distances at which TC retrieval is possible:

$$\zeta = \frac{-(c_x + c_y) \pm \sqrt{(c_x - c_y)^2 - 4}}{2(1 + c_x c_y)}. \tag{3.9}$$

It is evident that for $\zeta$ to have real and positive values, the following condition must be satisfied:

$$|c_x - c_y| \geq 2.$$

## 3.1 Diffraction from an Astigmatic Grating

The transmission function of an astigmatic grating is given by [28]

$$t(\mathbf{r}) = \sum_{q=-\infty}^{+\infty} t_q \exp\left[i2\pi q\left(\frac{x}{d'} - \frac{y^2}{2\lambda f}\right)\right], \tag{3.10}$$

where the structure along the $x$-direction acts as a standard linear grating with period $d'$. Along the $y$-direction, the quadratic phase term in $y^2$ introduces curvature to the grating lines, characterized by $\gamma = \frac{d'}{2\lambda f}$ [25]. This curvature corresponds to a one-dimensional (1D) Fresnel lens with effective focal length $f$ for an incident beam of wavelength $\lambda$.

When an LG beam with azimuthally symmetric intensity passes through a cylindrical lens–as an astigmatism inducing element–focusing occurs only along one axis. The combination of the lens's quadratic phase with the transverse twisted phase of the beam generates elongated intensity fringes in the focal plane. Similarly, since an astigmatic grating applies a quadratic phase along a single axis, it can be modeled as a cylindrical lens with effective focal length $f = \frac{d'}{2\lambda\gamma}$. By comparing the transmission function of this grating with the general astigmatism expression in Eq. (3.6), the coefficients are obtained as $c_x = 0$ and $c_y = -\frac{qz_R}{f}$. Consequently, the optimal propagation distances for detecting the TC of the generated beam are given by

$$\zeta_q = \frac{qz_R}{2f}\left[1 \pm \sqrt{1 - \left(\frac{2f}{qz_R}\right)^2}\right]. \tag{3.11}$$

The negative-sign solution is denoted as $z_1$ and the positive-sign solution as $z_2$. Here, $z_R = \pi 8 p w_b^2/\lambda$, and $q$ is the diffraction order of the astigmatic grating. Since $z_2$ is always much larger than $z_1$, subsequent analyses focus on the region near $z_1$. For instance, using $l = 5$ and Bessel scale parameter $w_b = 0.1\,\mathrm{mm}$ for the BGVB, along with grating period $d' = 0.1\,\mathrm{mm}$ and focal length $f = 70\,\mathrm{cm}$ (as in Fig. 5(a)), Eq. (3.11) yields $z_2 = 3.1 \times 10^5\,\mathrm{m}$. Figure 5(a) shows the first-order diffraction pattern of a BGVB after passing through the

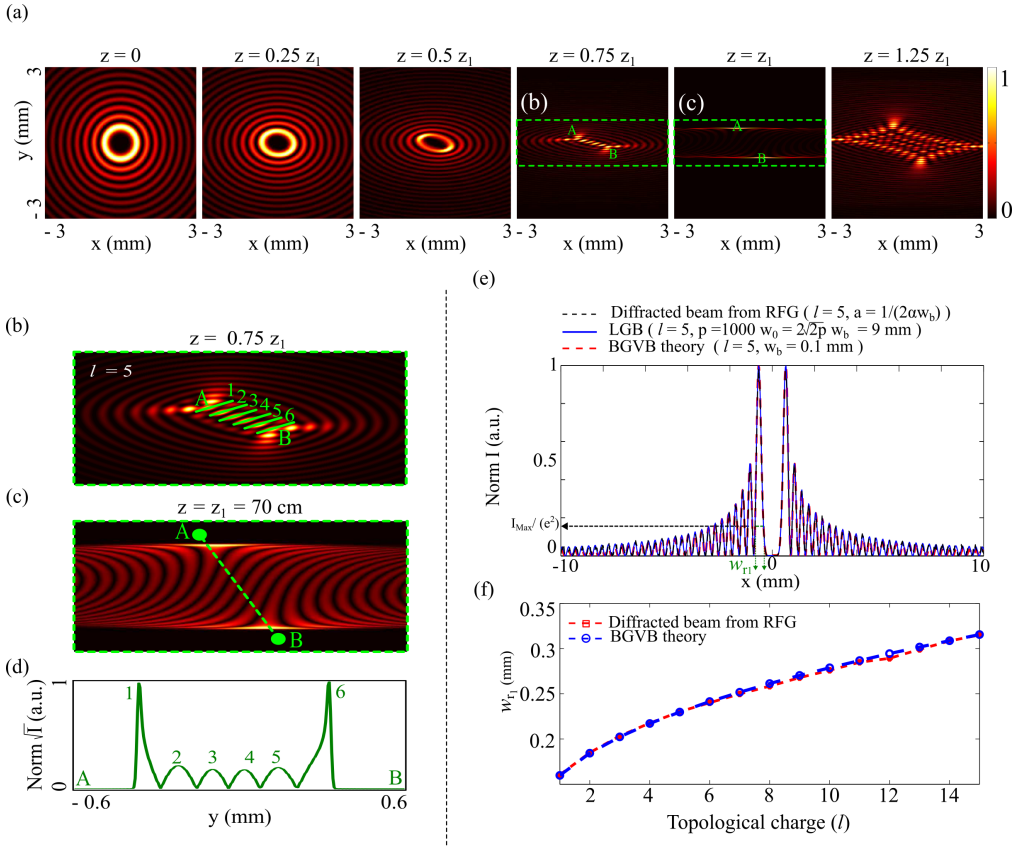


Figure 5: (a) First-order diffraction pattern of a BGVB with $l = 5$ and $w_b = 0.1\,\mathrm{mm}$ after passing through an astigmatic grating with period $d' = 0.1\,\mathrm{mm}$ and focal length $f = 70\,\mathrm{cm}$. The input beam is approximated as an LG beam with radial index $p = 1000$ and effective width $w_{0LG} = \sqrt{8p}\,w_b$. (b) and (c) Magnified views of the selected region in (a) at propagation distances $z = 0.75 z_1$ and $z = z_1$, respectively; in (c) the intensity is plotted using a square-root scale for clarity. (d) Transverse intensity profile along the dashed line in (c) for TC determination by counting peaks. (e) Comparison of transverse profiles for the theoretical BGVB, the equivalent LG beam, and the BGVB generated with an RFG hologram. (f) Comparison of the first-ring width of the theoretical BGVB and the RFG-generated BGVB as a function of TC.

astigmatic grating. In this simulation, the BGVB is approximated by an LG beam with radial index $p = 1000$ and effective width $w_{0LG} = \sqrt{8p}\,w_b$ (cf. Eq. (3.5)). Panels (b) and (c) show magnifications of the green-boxed region in (a) at propagation distances $z = 0.75 z_1$ and $z = z_1$, respectively. In (c), the intensity is plotted on a square-root scale to enhance visibility. At the theoretically optimal distance $z = z_1$ for TC retrieval, astigmatism induced

by the grating curvature elongates the intensity distribution, producing prominent bright streaks. Panel (d) shows the transverse intensity profile along the green dashed line in (c), where counting the number of peaks allows the TC $l$ to be determined. Even at shorter distances, e.g., $z = 0.75z_1$, where only the central ring is stretched by astigmatism, $l$ can still be determined from the central spots. As discussed previous section, the phase (or argument) of the BGVB generated in the $\pm m$-th diffraction order of an RFG hologram is given by the Bessel function $J_{\pm m\ell}\big(2\alpha r_0 r'_{\pm m}\big)$ (Eq. (2.10)). To facilitate comparison with the Bessel function appearing in the theoretical expression for the BGVB in Eq. (3.1), we introduce several simplifications. By placing the coordinate origin at the center of the hologram and aligning the propagation axis $z$ with the $m = +1$ diffraction order, the angular dependence is eliminated, and the radial coordinate can be approximated as follows:

$$r'_{+1} \approx \sqrt{r'^2 + \Big(\frac{\kappa_{+1}}{2\alpha}\Big)^2 + \frac{\kappa_{+1} r'}{\alpha}} \approx r' + \frac{\lambda z'}{d}.$$

In the far-field (Fraunhofer) regime, where $r' \gg \lambda z'/d$ - or equivalently, where the observation distance $r'$ significantly exceeds the characteristic transverse scale of the input beam ($w_0$)- the radial coordinate in the +1-st diffraction order simplifies to $r'_{+1} \approx r'$. This allows a direct comparison between the expressions:

$$J_{+l}\big(2\alpha r_0 r'_{+1}\big) \quad \text{and} \quad J_l\big(\frac{r'}{w_b}\big),$$

which leads to the relation

$$r_0 \approx \frac{1}{2\alpha w_b}.$$

In Fig. 5(e), we compare the transverse intensity profiles of three beams: the theoretical BGVB described by Eq. (3.1), the equivalent LG beam characterized by $p = 1000$ and $w^2_{0\mathrm{LG}} = 8p\, w_b^2$ (with $w_b = 0.1\,\mathrm{mm}$, see Eq. (3.5)), and the BGVB generated using an RFG hologram with an effective ring radius $r_0 \approx 1/(2\alpha w_b)$. As shown, the intensity distributions of all three beams exhibit excellent agreement. Figure 5(f) presents the variation of the first-ring width of the BGVB, obtained from both the theoretical BGVB and the RFG-generated beam, as a function of the beam TC. The results show excellent agreement between the two approaches. In Fig. 6, the diffraction patterns of the theoretical BGVB described by Eq. (3.1) (first column) are compared with those of the BGVBs generated using an RFG hologram (columns 2-4) after propagation through an astigmatic grating with focal length $f = 70\,\mathrm{cm}$ at various distances. In all cases, the parameters are $l = 5$ and $w_b = 0.1\,\mathrm{mm}$. The first column second row corresponds to the optimal distance for TC retrieval at $z = z_1$, where the elongated intensity streaks appear clearly, as expected.

For BGVBs generated by the diffraction of a Gaussian beam through an RFG hologram and subsequently passed through an astigmatic grating, as shown in the second and third columns of Fig. 6, when the distance between the hologram and the astigmatic grating is $z' = 10$ m, the optimal detection distance for the TC retrieval - i.e., the propagation distance at which the elongated intensity streaks are well formed - is $z = 1.07z_1$. However, when this distance is increased to $z' = 50$ m, the optimal detection distance becomes exactly $z = z_1$. This behavior occurs because, in the diffraction of a Gaussian beam by an RFG hologram, increasing the propagation distance before the astigmatic grating causes the optimal TC-retrieval plane to converge toward $z = z_1$. Consequently, after transmission through the astigmatic grating, the TC can be retrieved at a more precisely defined propagation distance.

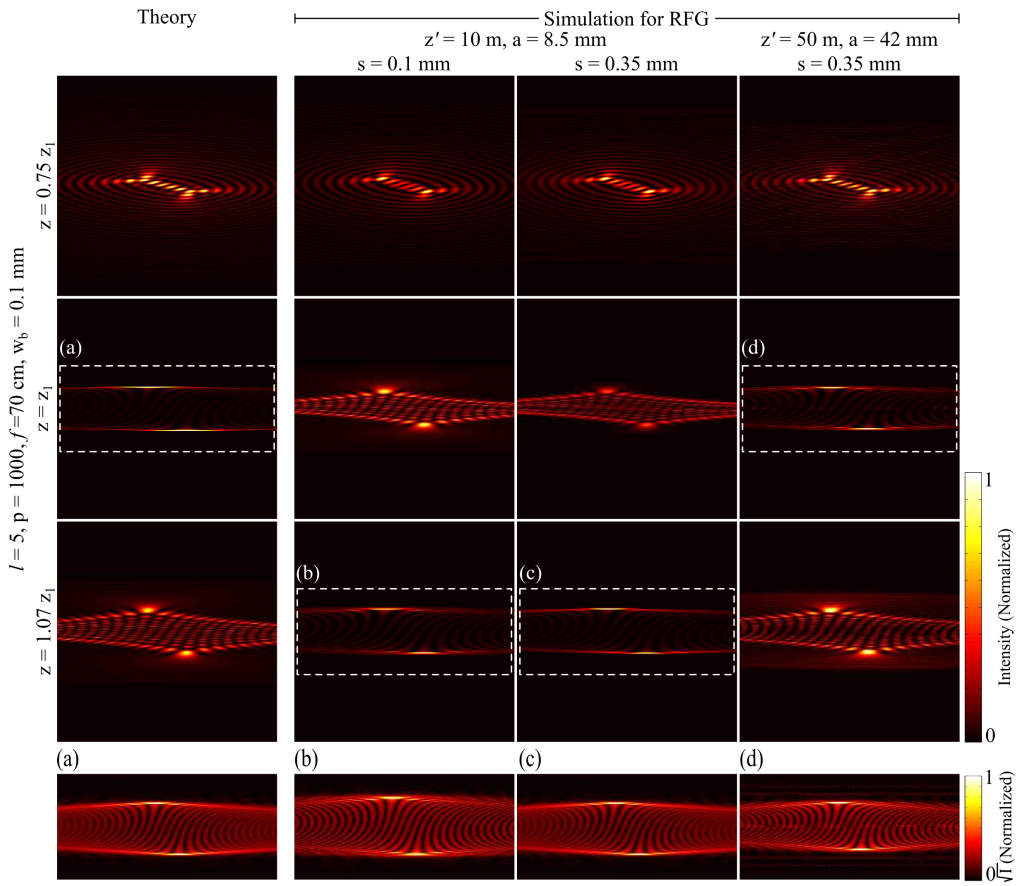


Figure 6: Comparison of the diffraction patterns of a theoretical BGVB (Eq. (3.1)) after passing through an astigmatic grating with those of two RFG-generated BGVBs (with different values of $s$), shown at three propagation distances. For the ideal beam (first column), the elongated intensity distribution appears clearly at $z = z_1$. In the second and third columns, corresponding to the RFG-generated BGVBs, this elongated pattern forms near $z = 1.07z_1$ when the hologram–grating distance is short ($z' = 10\,\mathrm{m}$). Increasing this distance to 50 m shifts the elongated pattern to $z = z_1$, in agreement with the theoretical prediction.

# 4 Experimental Measurements

The experimental setup used for the generation and characterization of BGVBs is schematically shown in Fig. 7(a). A diode-pumped Nd:YAG laser operating at a wavelength of $\lambda = 532$ nm served as the light source. The output beam was first directed through a spatial filter (consisting of a microscope objective and a pinhole) to improve its spatial quality. The filtered and expanded beam was then collimated using a lens system before being incident on a binary pure-amplitude RFG hologram fabricated lithographically on a glass substrate. The RFG parameters were set to an inner radius $a = 0.9\,\mathrm{mm}$, ring width $s = 0.1\,\mathrm{mm}$, and fundamental TC $l = +2$.

During propagation, BGVBs with $l = +2$ are generated in the first diffraction orders, while higher diffraction orders carry higher TCs. One of these nonzero diffraction orders is selected for further propagation, and all other orders are blocked. The resulting BGVB then

passes through an astigmatic amplitude grating with period $d = 0.1\,\text{mm}$ and $\gamma = 0.04\,\text{mm}^{-1}$. The diffraction pattern in the positive first order of the grating is recorded using a Nikon D7200 camera.

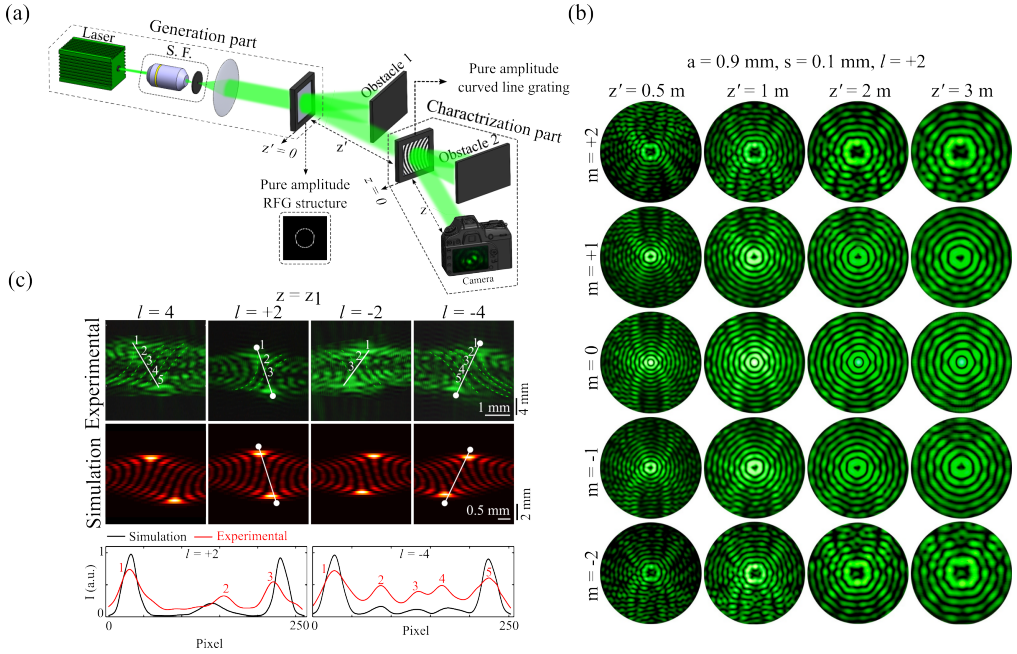


Figure 7: (a) Schematic of the experimental setup. A Nd:YAG laser at 532 nm is collimated and directed onto the RFG hologram. A selected diffraction order is allowed to propagate through an astigmatic grating, and the resulting diffraction pattern is recorded by a camera. (b) Diffraction patterns from different orders of the RFG hologram with inner radius $a = 0.9\,\text{mm}$, ring width $s = 0.1\,\text{mm}$, and TC $l = +2$, captured at various propagation distances. (c) Diffraction patterns of the BGVBs generated in different diffraction orders of the RFG hologram after passing through the astigmatic grating and recorded in the positive first order at $z = z_1$. The input beams correspond to diffraction orders $m = \pm 1$ and $m = \pm 2$ of the binary RFG with fundamental TC $l = 2$, producing vortices of charges 2 and 4, respectively. The recording camera is positioned at $z = z_1$ from the astigmatic grating. Green patterns (first row) show experimental results, while red patterns (second row) show simulations. In the third row, 1D intensity profiles of the beams along the white lines are plotted for the beams with TCs $l = +2$ and $l = -4$. The red plots correspond to the experimental results, and the black plots correspond to the numerical simulations.

Figure 7(b) presents the BGVBs generated in different diffraction orders of the binary RFG hologram with fundamental TC $l = +2$, recorded at various propagation distances. Here, $m$ denotes the diffraction order of the RFG hologram. The TC in each order is given by $l_m = m \times l$. For instance, for a binary RFG with fundamental TC $l = +2$, the beam in the diffraction order $m = -2$ carries a TC of $l_m = -4$.

Figure 7(c) shows a comparison between the experimental and simulated diffraction patterns in the positive first diffraction order of the astigmatic grating at $z = z_1 = 2.5\,\text{m}$. These patterns correspond to BGVBs generated in the diffraction orders $m = \pm 1$ and $m = \pm 2$ of the binary RFG with TC $l = +2$. The RFG hologram is positioned at $z' = 3.8\,\text{m}$ from the astigmatic grating. The green patterns (first row) represent the experimental measure-

ments, while the red patterns (second row) show the numerical simulations, demonstrating excellent agreement. In the third row, the 1D intensity profiles extracted along the white lines are shown for the beams with TCs $l = +2$ and $l = -4$. The red plots correspond to the experimental results, and the black plots correspond to the numerical simulations. The same RFG structure used in panel (b) is employed for generating the BGVBs, and an astigmatic grating with curvature $\gamma = 0.04\,\mathrm{mm}^{-1}$ is used for beam characterization.

Figure 8(a) shows a picture of the constructed binary pure-amplitude RFG hologram which is used in the experiments. Figure 8(b) presents three binary-profile astigmatic gratings with different line curvatures, used to characterize the BGVBs generated in the first diffraction order of the RFG hologram with $l = +2$. The diffraction patterns presented in Fig. 8(c) were recorded at the propagation distance $z = z_1$. The results show that increasing the curvature of the grating lines compresses the diffraction pattern, effectively acting as a lens with a shorter focal length and producing elongated intensity fringes at a closer propagation distance. The same RFG structure shown in Fig. 7 is used here, with a separation of $z' = 3.8\,\mathrm{m}$ between the RFG and the astigmatic grating.

Figure 9 shows the modified intensity profile of a BGVB with $l = +2$, generated in the first diffraction order of the RFG and recorded at various propagation distances after passing through an astigmatic grating with curvature $\gamma = 0.04\,\mathrm{mm}^{-1}$. The parameters of both the RFG and the grating are identical to those used in Fig. 8. The experimental results demonstrate that, when using an astigmatic grating to characterize BGVBs, the elongated intensity fringes appear distinctly at $z = z_1$, in good agreement with numerical simulations. The TC of the BGVB can be determined by counting the number of bright elongated fringes ($N = 3$) at this distance, yielding $l = N - 1 = 2$.

# 5 Conclusions

We have proposed and demonstrated a novel holographic approach for generating Bessel-Gaussian vortex beams (BGVBs) using a fork grating multiplied by a ring-shaped transmission function. The incorporation of a helical phase within the grating structure enables the production of vortex light in the first diffraction order, while the ring aperture ensures the formation of a BGVB intensity distribution in the far field. The fabricated structure, realized through lithography on a glass substrate, successfully produced reasonable-quality BGVBs when illuminated by a Gaussian beam. In this work, the effect of the ring width and radius on the quality and propagation behavior of the generated beams was theoretically investigated. In addition, a theoretical relation was derived to determine the optimal distance at which the annular input intensity distribution transforms into elongated bright fringes after passing through the astigmatic grating. This optimal distance was expressed as a function of the astigmatic grating curvature, the illuminating wavelength, and the grating period, enabling precise prediction of the observation plane required for TC characterization. The purposed method offers a compact platform for generating BGVBs, enabling potential applications in optical communications, particle manipulation, and advanced imaging systems.

# Authors' Contributions

SR conceptualized and supervised the research; established the methodology; provided a physical interpretation of the observations; validated the results; secured funding; managed the project; and provided resources. SR, SF, and PA collaboratively set up the experimental

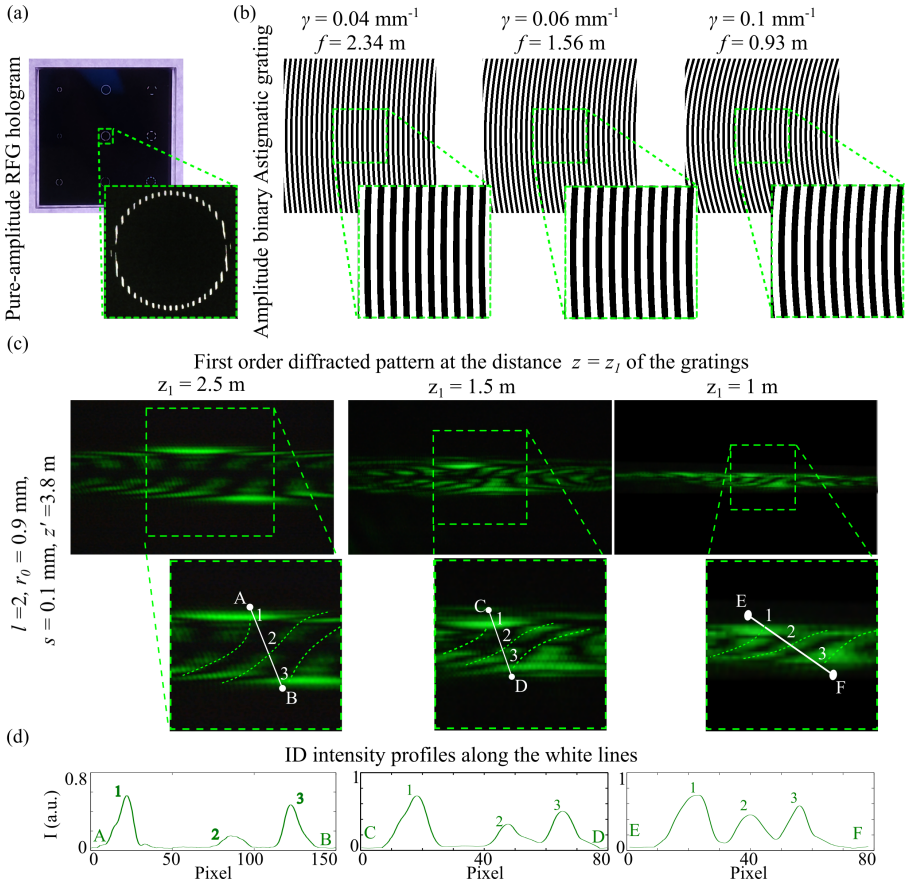


Figure 8: (a) A picture of the constructed binary pure-amplitude RFG hologram used in the experiments. (b) Binary-profile astigmatic gratings with different line curvatures, (c) the corresponding first-order diffraction patterns recorded at $z = z_1$, and (d) 1D intensity profiles of the beams along the white lines presented in the insets of (c). The illuminating BGVB is generated from the first diffraction order of an RFG with inner radius $a = 0.9\,\text{mm}$, ring width $s = 0.1\,\text{mm}$, and TC $l = +2$, under Gaussian-beam illumination.

apparatus and conducted the experiments with PA contributing specifically to the first stage of work. SR and SF presented the formulation, analyzed the data, performed investigations, and prepared the figures. SR wrote the manuscript. AAA reviewed the manuscript and validated the results.

## Data Availability

The manuscript has no associated data or the data will not be deposited.

## Conflicts of Interest

The author declares that there is no conflict of interest.

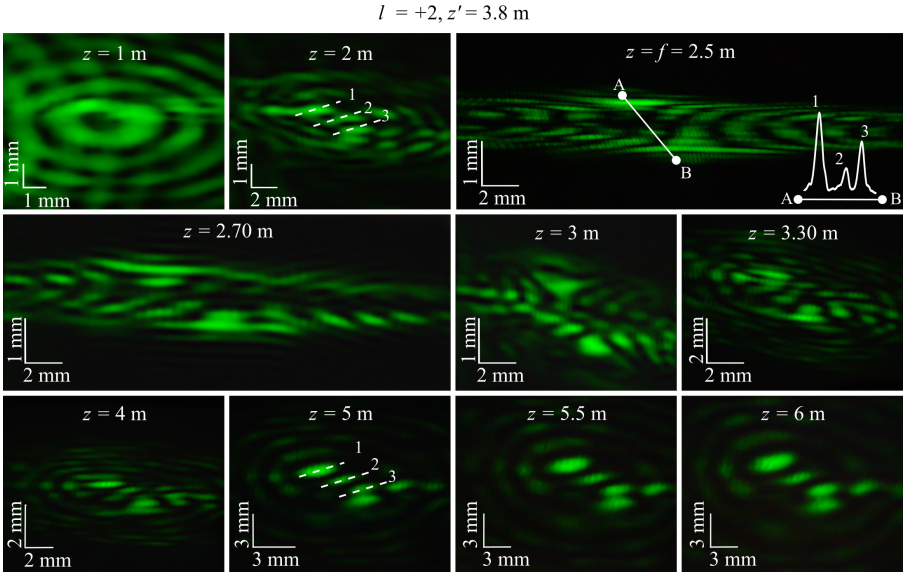


Figure 9: First-order diffraction patterns of a BGVB with $l = +2$ after passing through an astigmatic grating with curvature $\gamma = 0.04\,\mathrm{mm}^{-1}$, recorded at different propagation distances.

## Ethical Considerations

The author has diligently addressed ethical concerns, such as informed consent, plagiarism, data fabrication, misconduct, falsification, double publication, redundancy, submission, and other related matters. Iran National Science Foundation (4037535); Institute for Advanced Studies in Basic Sciences (G2025IASBS12632).

## Acknowledgment

This work is based upon research funded by Iran National Science Foundation (INSF) under project No.4037535.

## References

[1] M. S. Soskin and M. V. Vasnetsov, "Singular optics," Prog. Opt. **42**(4), 219 (2001). DOI: https://doi.org/10.1016/S0079-6638(01)80018-4

[2] X. Zhang, T. Xia, S. Cheng, and S. Tao, "Free-space information transfer using the elliptic vortex beam with fractional TC," Opt. Commun. **431**, 238 (2019). DOI: https://doi.org/10.1016/j.optcom.2018.09.035

[3] R. Steiger, S. Bernet, and M. Ritsch-Marte, "SLM-based off-axis Fourier filtering in microscopy with white light illumination," Opt. Express **20**(14), 15377 (2012). DOI: https://doi.org/10.1364/OE.20.015377

[4] T. Yu, H. Xia, W. Xie, G. Xiao, and H. Li, "The generation and verification of Bessel-Gaussian beam based on coherent beam combining," Results Phys. **16**, 102872 (2020). DOI: https://doi.org/10.1016/j.rinp.2019.102872

[5] K. Toyoda, K. Miyamoto, N. Aoki, R. Morita, and T. Omatsu, "Using optical vortex to control the chirality of twisted metal nanostructures," Nano Lett. **12**(7), 3645 (2012). DOI: https://doi.org/10.1021/nl301347j

[6] J. F. Nye and M. V. Berry, "Dislocations in wave trains," Proc. R. Soc. Lond. A Math. Phys. Sci. **336**(1605), 165 (1974). DOI: https://doi.org/10.1098/rspa.1974.0012

[7] M. V. Berry and M. R. Dennis, "Phase singularities in isotropic random waves," Proc. R. Soc. Lond. A Math. Phys. Eng. Sci. **456**(2001), 2059 (2000). DOI: https://doi.org/10.1098/rspa.2000.0602

[8] M. McLaren, M. Agnew, J. Leach, F. S. Roux, M. J. Padgett, R. W. Boyd, and A. Forbes, "Entangled Bessel-Gaussian beams," Opt. Express **20**(21), 23589 (2012). DOI: https://doi.org/10.1364/OE.20.023589

[9] Z. Zhi, Q. Na, Q. Xie, B. Chen, Y. Li, X. Liu, X. Li, L. Wang, G. Lo, and J. Song, "On-chip generation of Bessel-Gaussian beam via concentrically distributed grating arrays for long-range sensing," Light Sci. Appl. **12**(1), 92 (2023). DOI: https://doi.org/10.1038/s41377-023-01133-2

[10] X. Chu, Q. Sun, J. Wang, P. Lu, W. Xie, and X. Xu, "Generating a Bessel-Gaussian beam for the application in optical engineering," Sci. Rep. **5**, 18665 (2015). DOI: https://doi.org/10.1038/srep18665

[11] J. J. Durnin, J. J. Miceli Jr, and J. H. Eberly, "Diffraction-free beams," Phys. Rev. Lett. **58**(15), 1499 (1987). DOI: https://doi.org/10.1103/PhysRevLett.58.1499

[12] R. M. Herman and T. A. Wiggins, "Nondiffracting optical beams," Ferroelectrics, **131**(1), 119 (1992). DOI: 10.1080/00150199208223401

[13] J. Turunen, A. Vasara, and A. T. Friberg, "Holographic generation of diffraction-free beams," Appl. Opt., **27**(18), 3959 (1988). DOI: 10.1364/AO.27.003959

[14] A. Vasara, J. Turunen, and A. T. Friberg, "Realization of general nondiffracting beams with computer-generated holograms," J. Opt. Soc. Am. A **6**(11), 1748 (1989). DOI: https://doi.org/10.1364/JOSAA.6.001748

[15] Z. Zhai, Z. Cheng, Q. Lv, and X. Wang, "Tunable axicons generated by spatial light modulator with high-level phase computer-generated holograms," Appl. Sci. **10**(15), 5127 (2020). DOI: https://doi.org/10.3390/app10155127

[16] M. Harris, C. A. Hill, P. R. Tapster, and J. M. Vaughan, "Laser modes with helical wave fronts," Phys. Rev. A **49**(4), 3119 (1994). DOI: https://doi.org/10.1103/PhysRevA.49.3119

[17] J. Arlt and K. Dholakia, "Generation of high-order Bessel beams by use of an axicon," Opt. Commun. **177**(1–6), 297 (2000). DOI: https://doi.org/10.1016/S0030-4018(00)00572-1

[18] C.-S. Guo, L.-L. Lu, and H.-T. Wang, "Characterizing TC of optical vortices by using an annular aperture," Opt. Lett. **34**(23), 3686 (2009). DOI: https://doi.org/10.1364/OL.34.003686

[19] J. M. Hickmann, E. J. S. Fonseca, W. C. Soares, and S. Chavez-Cerda, "Unveiling a truncated optical lattice associated with a triangular aperture using light's orbital angular momentum," Phys. Rev. Lett. **105**(5), 053904 (2010). DOI: https://doi.org/10.1103/PhysRevLett.105.053904

[20] D. Hebri, S. Rasouli, and A. M. Dezfouli, "Theory of diffraction of vortex beams from structured apertures and generation of elegant elliptical vortex Hermite–Gaussian beams," J. Opt. Soc. Am. A **36**(5), 839 (2019). DOI: https://doi.org/10.1364/JOSAA.36.000839

[21] I. Moreno, J. A. Davis, B. M. L. Pascoguin, M. J. Mitry, and D. M. Cottrell, "Vortex sensing diffraction gratings," Opt. Lett. **34**(19), 2927 (2009). DOI: https://doi.org/10.1364/OL.34.002927

[22] S. Topuzoski and L. Janicijevic, "Conversion of high-order –Gaussian beams into Bessel beams of increased, reduced or zeroth order by use of a helical axicon," Opt. Commun. **282**(17), 3426 (2009). DOI: https://doi.org/10.1016/j.optcom.2009.05.052

[23] K. Dai, C. Gao, L. Zhong, Q. Na, and Q. Wang, "Measuring OAM states of light beams with gradually-changing-period gratings," Opt. Lett. **40**(4), 562 (2015). DOI: https://doi.org/10.1364/OL.40.000562

[24] D. Hebri, S. Rasouli, and M. Yeganeh, "Intensity-based measuring of the TC alteration by the diffraction of vortex beams from amplitude sinusoidal radial gratings," J. Opt. Soc. Am. B **35**(4), 724 (2018). DOI: https://doi.org/10.1364/JOSAB.35.000724

[25] P. Amiri, A. M. Dezfouli, and S. Rasouli, "Efficient characterization of optical vortices via diffraction from parabolic-line linear gratings," J. Opt. Soc. Am. B **37**(9), 2668 (2020). DOI: https://doi.org/10.1364/JOSAB.398143

[26] S. Rasouli, P. Amiri, V. V. Kotlyar, and A. A. Kovalev, "Characterization of a pair of superposed vortex beams having different winding numbers via diffraction from a quadratic curved-line grating," J. Opt. Soc. Am. B **38**(8), 2267 (2021). DOI: https://doi.org/10.1364/JOSAB.428390

[27] S. Rasouli, S. Fathollazade, and P. Amiri, "Simple, efficient and reliable characterization of Laguerre-Gaussian beams with non-zero radial indices in diffraction from an amplitude parabolic-line linear grating," Opt. Express **29**(19), 29661 (2021). DOI: https://doi.org/10.1364/OE.435116

[28] S. Fathollazade, S. Rasouli, D. Hebri, P. Amiri, and S. A. Ponomarenko, "Laguerre–Gaussian-to-Hermite–Gaussian mode conversion revisited," J. Opt. Soc. Am. A **42**(4), 495 (2025). DOI: https://doi.org/10.1364/JOSAA.547816

[29] L. Janicijevic and S. Topuzoski, "Fresnel and Fraunhofer diffraction of a Gaussian laser beam by fork-shaped gratings," J. Opt. Soc. Am. A **25**(11), 2659 (2008). DOI: https://doi.org/10.1364/JOSAA.25.002659

[30] J. Kowalczyk, S. N. Smith, and E. B. Szarmes, "Generation of Bessel beams using a 4-f spatial filtering system," Am. J. Phys. **77**(3), 229 (2009). DOI: https://doi.org/10.1119/1.3033743

[31] M. Abramowitz, I. A. Stegun, and R. H. Romer, "Handbook of mathematical functions with formulas, graphs, and mathematical tables," Am. Assoc. Phys. Teachers (1988).

[32] M. Abramowitz and I. Stegun, "Handbook of Mathematical Functions", 3rd ed. (Dover, New York, NY, USA, 1972).

[33] A. E. Siegman, "Lasers", University Science Books, (1986).

[34] A. Wada, T. Ohtani, Y. Miyamoto, and M. Takeda, "Propagation analysis of the Laguerre–Gaussian beam with astigmatism," J. Opt. Soc. Am. A **22**(12), 2746 (2005). DOI: https://doi.org/10.1364/JOSAA.22.002746